Compact Models for Memristors Based on Charge–Flux Constitutive Relationships

Sangho Shin, *Member, IEEE,* Kyungmin Kim, *Member, IEEE,* and Sung-Mo Kang, *Fellow, IEEE*

***Abstract*—This paper introduces compact models for memristors. The models are developed based on the fundamental constitutive relationships between charge and flux of memristors. The modeling process, with a few simple steps, is introduced. For memristors with limited resistance ranges, a simple method to find their constitutive relationships is discussed, and examples of compact models are shown for both current-controlled and voltage-controlled memristors. Our models satisfy all of the memristor properties such as frequency dependent hysteresis behaviors and also unique boundary assurance to simulate memristors whether they behave memristively or resistively. Our models are implementable in circuit simulators, including SPICE, Verilog-A, and Spectre.**

***Index Terms*—Constitutive relationship, macromodel, memductor, memristor, Spectre, SPICE, Verilog-A.**

I. Introduction

AFTER Williams *et al.* of Hewlett-Packard (HP), Palo Alto, CA, reported a physical realization and understanding of memristors and memristor's switching mechanism in 2008 [1], [2], research efforts related to memristors have been growing rapidly throughout the world. Besides the immediate application to nonvolatile resistive memories [3], researchers have suggested to build memristor-based ultrahigh density Boolean logic gates without active transistors [4]. In addition, memristors may be used for neuromorphic applications to simulate learning, adaptive, and spontaneous behaviors [5]–[9]. Recently, Shin *et al.* [10] reported that memristors can be used to program differential analog circuits continuously by patterning input voltage or current waveforms.

In order to help research efforts to overcome the current circuit design challenges with use of memristors, this paper introduces constitutive relationship-based new compact models of memristors which can be easily implemented in circuit simulation tools such as SPICE, Spectre, Verilog-A, and so on. A physical model-based method of modeling such devices has been recently reported, a method that is comprised of resistive ports and memory sections [11]–[13]. This approach was utilized for SPICE modeling of the memristor reported in [1], and considers nonlinear dopant drift effect which appears around the limiting boundary resistances [1], [11], [13]. However, this modeling method cannot be used for a device that lacks detailed physical equations, since the approach is basically a circuit realization of the physical model.

Unlike the recently reported modeling methods of memristor [11]–[13], our modeling approach is uniquely based on the constitutive relationship of memristors between charge and flux. Since a memristor provides a unique constitutive relationship by its definition, our modeling method can be applied to any memristor device, regardless of whether it possesses its physical equations or not, and the model parameters can be easily extracted from measured constitutive relationships.

As for the organization of this paper, in Section II, we will describe our constitutive relationship-based modeling approach. Then we will discuss how the constitutive relationship can be found for memristors with limited memristance range in Section III. Section IV will present macromodels for both current-controlled and for voltage-controlled memristors. Finally, examples of model parameter extraction and simulation results will be shown in Section V, followed by discussions regarding specific limitations of our models and additional consideration for modeling of the nonlinear dopant drift effect in Section VI.

II. Compact Modeling for Memristors

Memristor was originally defined in 1971 by Chua [14] to represent the missing constitutive relationship between charge (q) and flux (φ), by assuming the relationship as $\varphi = f(q)$. From the relationship, the memristance can be derived mathematically by taking time derivatives on both sides

$$\frac{d\varphi}{dt} = \frac{d}{dt}\left[f(q)\right] = \left\{\frac{d}{dq}f(q)\right\} \cdot \frac{dq}{dt} \tag{1a}$$

$$v_M = \left\{\frac{d}{dq}f(q)\right\} \cdot i_M \equiv R_M(q) \cdot i_M. \tag{1b}$$

Equation (1a) is deduced to (1b) when the relationships between flux and voltage ($v = d\varphi/dt$), as well as charge and current ($i = dq/dt$) are invoked, where $R_M(q)$ is the memristance defined by a derivative of the charge–flux relationship with respect to the charge, i.e., $R_M(q) = df(q)/dq$. And thus, any device which can present its resistance as $R_M(q)$ can be called as a current-controlled memristor. Here, it should be noted that memristance values can be uniquely found by

Manuscript received July 24, 2009; revised October 13, 2009. Current version published March 19, 2010. This work was supported in part by the University of California, Merced. This paper was recommended by Associate Editor, K. Chakrabarty.

The authors are with the School of Engineering, University of California, Merced, CA 95343 USA (e-mail: sshin8@ucmerced.edu; kkim35@ucmerced.edu; smk123@ucmerced.edu).

Color versions of one or more of the figures in this paper are available online at http://ieeexplore.ieee.org.

Digital Object Identifier 10.1109/TCAD.2010.2042891

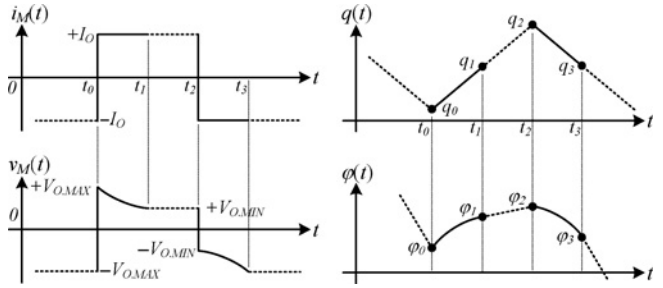

Fig. 1. Example of transient v–i waveforms and corresponding charge (q) and flux (φ) waveforms of a memristor, where the memristor's memristive regions, $t = [t_0, t_1]$ and $t = [t_2, t_3]$, are plotted in solid line and its resistive regions are depicted in dashed line.

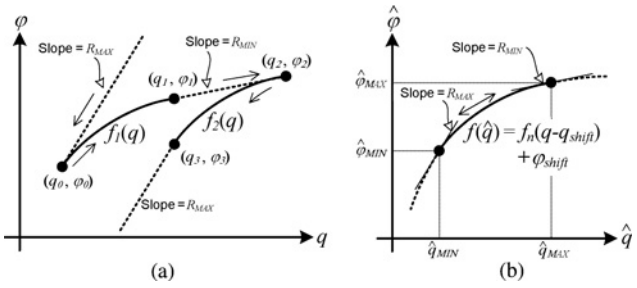

Fig. 2. Charge–flux relationships. (a) Actual relations corresponding to the waveforms in Fig. 1. (b) Memristive equivalent relationship with shifts and an introduction of window function of (3a) on i_M.

measuring slopes, once the constitutive φ–q relationship is offered.

Similar to the current-controlled memristor, a voltage-controlled memductor (short for memory conductor) can be defined by a charge–flux constitutive relationship, i.e., $q = g(\varphi)$. Taking time derivatives on both sides renders

$$\frac{dq}{dt} = \frac{d}{dt}\left[g(\varphi)\right] = \left\{\frac{d}{d\varphi}g(\varphi)\right\} \cdot \frac{d\varphi}{dt} \tag{2a}$$

$$i_M = \left\{\frac{d}{d\varphi}g(\varphi)\right\} \cdot v_M \equiv G_M(\varphi) \cdot v_M \tag{2b}$$

where $G_M(\varphi)$ is termed a voltage-controlled memductance values which can be uniquely found by measuring slopes of the charge–flux relationship of $g(\varphi)$, i.e., $G_M(\varphi) = dg(\varphi)/d\varphi$.

When we use the above constitutive relationship-based memristance representation, circuit models for memristors can be found in compact model forms. However, when we consider a boundary condition that a memristor behaves memristively only within a bounded resistance range between R_{MIN} and R_{MAX}, i.e., $R_M \in [R_{\mathrm{MIN}}, R_{\mathrm{MAX}}]$, $f(q)$ and $g(\varphi)$ need to be redefined as $f(\hat{q})$ and $g(\hat{\varphi})$ in a model space, because the constitutive relationships are valid only in the memristive region, while the actual device can behave as a linear resistor at the two boundary resistances. Within the secondary boundary conditions of $\hat{q} \in \left[\hat{q}_{\mathrm{MIN}}, \hat{q}_{\mathrm{MAX}}\right]$ and $\hat{\varphi} \in [\hat{\varphi}_{\mathrm{MIN}}, \hat{\varphi}_{\mathrm{MAX}}]$, our modeling approach for memristors can be summarized as follows, since the R_M $(\hat{q})$ and $G_M(\hat{\varphi})$ can be easily derived by taking slopes once $f(\hat{q})$ and g$(\hat{\varphi})$ are found.

1) Extract $f(\hat{q})$, or $g(\hat{\varphi})$, from v–i measurements.
2) Extract R_M $(\hat{q})$, or $G_M(\hat{\varphi})$ by taking their slopes.
3) Represent by circuit $v_M = R_M(\hat{q}) \cdot i_M$ or $i_M = G_M(\hat{\varphi}) \cdot v_M$.

In the next section, we will describe how the charge–flux constitutive relationships of memristors with limited resistance range can be found.

III. Charge−Flux Constitutive Relationship

Due to the memristor's limited resistance range, the device must be confined to the available range. Once the device resistance reaches either boundary value, it will remain at the boundary resistance value when the excess charge or flux is applied to the device. Fig. 1 shows example waveforms of a memristor with its limited resistance range, where the input current is patterned to transition to $+I_O$ from $-I_O$ at t_0 and back to $-I_O$ at t_2. Assuming that the memristance starts to change its value from R_{MAX} at t_0 and it eventually becomes equal to R_{MIN} at t_1, the corresponding charge and flux waveforms are shown in the right hand side of Fig. 1, where the memristive and resistive operations are depicted in solid lines and dashed lines, respectively. Regarding the φ–q relationship depicted in Fig. 2(a), it can be noted that the piecewise φ–q functions, $f_1(q)$ and $f_2(q)$, of each memristive region are fully correlated each other with shifts in q-axis and φ-axis, i.e., $f_2(q) = f_1(q - q_{shift}) + \varphi_{shift}$. It means that a memristive charges and flux $(\hat{\varphi} - \hat{q})$ relation can be uniquely defined as $\hat{\varphi} = f(\hat{q}) = f_n(q - q_{shift})$ from any of the piecewise memristive φ–q functions.

However, in order to ensure that the boundary limits are not violated at the hard switching conditions with boundary resistance values, the excess input current (or voltage) in the resistive regions should be disregarded. In other words, the input current (or voltage) should be masked in the model by a function (H) so that the $\hat{q}$ (or $\hat{\varphi}$) can be always within the memristive regions of $f(\hat{q})$, whether memristors behave memristively or resistively. A masked input current $(\hat{i}_M)$ of current-controlled memristors is defined as

$$\hat{i}_M = H(i_M) = \begin{cases} i_M, & \text{if } R_M \in (R_{\mathrm{MIN}}, R_{\mathrm{MAX}}) \\ 0, & \text{else if } i_M \text{ does not pass zero.} \end{cases} \tag{3a}$$

Similarly, a masked input voltage of voltage-controlled memristors can be defined as

$$\hat{v}_M = H(v_M) = \begin{cases} v_M, & \text{if } R_M \in (R_{\mathrm{MIN}}, R_{\mathrm{MAX}}) \\ 0, & \text{else if } v_M \text{ does not pass zero.} \end{cases} \tag{3b}$$

Equations (3a) and (3b) mean that any excess current (or voltage) application in resistive region will be disregarded in the model space. When the memristance is considered, the equations are valid since any amount of excess current (or voltage) application in the resistive region will not affect the memristance anymore as long as the input polarity is not negated. Once it hits either of the boundary resistance values, it holds to its boundary value regardless of the input amplitude for the same polarity. In terms of device behavior, memristors will move back into the memristive region as soon as the input polarity is reversed so that $\hat{i}_M$(or $\hat{v}_M$) can reflect the input current (or voltage) of its memristive operation. These phenomena are analogous to that of a charge reservoir with

limited capacity, thus siphoning excess currents beyond its capacity. Interestingly, the masking function behaves exactly same as an ideal diode, which clips input potentials higher than its threshold value.

Equations (3a) and (3b) are contained by the secondary boundary conditions of $\hat{q} \in [\hat{q}_{\mathrm{MIN}}, \hat{q}_{\mathrm{MAX}}]$ and $\hat{\varphi} \in [\hat{\varphi}_{\mathrm{MIN}}, \hat{\varphi}_{\mathrm{MAX}}]$, the memristive charge and flux, respectively. Considering that any shifts of $f(\hat{q})$ and $g(\hat{\varphi})$ either in $\hat{q}$-axis or in $\hat{\varphi}$-axis are allowed without affecting the memristance, we can choose any value for $\hat{q}_{\mathrm{MIN}}$ and $\hat{\varphi}_{\mathrm{MIN}}$ so that the mathematical representations for $f(\hat{q})$ and $g(\hat{\varphi})$ can be in simplest forms.

Once the $f(\hat{q})$ and $g(\hat{\varphi})$ are chosen, with limited ranges of $\hat{q} \in [\hat{q}_{\mathrm{MIN}}, \hat{q}_{\mathrm{MAX}}]$ and $\hat{\varphi} \in [\hat{\varphi}_{\mathrm{MIN}}, \hat{\varphi}_{\mathrm{MAX}}]$, the initial conditions for $\hat{q}$ and $\hat{\varphi}$ which correspond to the initial memristance (r_{mo}), are determined so that $R_M(\hat{q}_o) = r_{\mathrm{mo}}$ and $G_M(\hat{\varphi}_o) = 1/r_{\mathrm{mo}}$, respectively.

IV. Memristor Models

As described in the previous section, a compact model of memristors for circuit design and simulation can be easily formed by using the unique constitutive relationships between charge and flux. Since the charge–flux relationship of a memristor can be easily found by measuring the transient voltage output under a periodic input current pattern, or by measuring the transient current output under the patterned input voltage, our constitutive relationship-based modeling approach can significantly reduce the modeling complexity.

A. Current-Controlled Memristors

In this section, a constitutive relationship-based model for current-controlled memristors will be introduced. In general, a time-invariant memristive system can be expressed by (15) and (16). When the memristance R_M is assumed to be dependent only on its internal state variable x which incorporates memory effects and is controlled by input i_M, the system can be expressed by the following equations:

$$v_M = R_M(x) \cdot i_M \tag{4a}$$

$$x' = \frac{dx}{dt} = r(x, i_M) \tag{4b}$$

where $r(\cdot)$ is an input controlled rate function of the state variable x. The most challenging problem with this representation is that the state variable x is usually not available for physical measurements. Recently, researchers with HP have presented that a dopant penetration in time in a thin film nanoscale memristor could be the state variable which primarily determines the device's memristance [1]. Despite the fact that their model well identifies its physical meaning, the dopant penetration, as a state variable, is still difficult to handle for model parameter extraction.

For physical measurability and simplicity, we will use the memristance itself as the state variable in this paper, i.e., $R_M(x) = x$, and then the rate function $r(\cdot)$ becomes a memristance change rate. Considering that the memristance x is a function of charges with a relation of $x = df(\hat{q})/d\hat{q}$, the rate function $r(\cdot)$ should be equal to the following equation:

$$x' = \frac{dx}{dt} = \frac{dx}{d\hat{q}} \cdot \frac{d\hat{q}}{dt} = \frac{dx}{d\hat{q}} \cdot \hat{i}_M = \left\{ \frac{d^2}{d\hat{q}^2} f(\hat{q}) \right\} \cdot \hat{i}_M \tag{5}$$

where $\hat{i}_M$is the masked input current by (3a). From (5), we discern that the constitutive relationship between charge and flux holds many meaningful features. Besides the most distinct feature that the slopes of $f(\hat{q})$ is equal to the instantaneous memristance x, the second derivative of $f(\hat{q})$ with respect to $\hat{q}$ is a term proportional to the rate of the memristance change. (The first derivative is memristance, the second derivative is acceleration of the memristance change rate.) Thus, we can extract all required functions from $f(\hat{q})$, for any kind of memristor representations.

We have already shown in the previous section, how $f(\hat{q})$ can be found from simple device measurements. However, in this model example, we use a derived $f(\hat{q})$ from HPs model which includes a state variable w, since no measurable memristor device is currently available. HP researchers reported their memristor model as the following coupled (6a) and (6b) [1], where w, μ_v, and D denote a state variable, average carrier mobility, and device thickness, respectively

$$v_M = \left\{ R_{\mathrm{MIN}} \frac{w}{D} + R_{\mathrm{MAX}} \left(1 - \frac{w}{D}\right) \right\} \cdot i_M \tag{6a}$$

$$w' = \frac{dw}{dt} = \alpha \cdot \mu_v \frac{R_{\mathrm{MIN}}}{D} \cdot \hat{i}_M \tag{6b}$$

where we added a scaling factor (α) to the second equation. Though the scaling factor α is not an essential parameter, it is added to provide model programmability and to easily model even much more enhanced device with fast resistance change rate, since the memristance change rate is proportional to α. As for the input current, a masked current ($\hat{i}_M$) defined by (3a) is used for the second equation. It is valid because the state variable w can be modulated only within its memristive region and w will no longer change with the same input polarity once it hits either of the boundaries of $w \in [0, D]$.

With $x \equiv \{R_{\mathrm{MIN}}(w/D) + R_{\mathrm{MAX}}(1 - w/D)\}$, the above coupled device equations can be rewritten as

$$v_M = x \cdot i_M \tag{7a}$$

$$x' = \gamma \cdot \hat{i}_M \tag{7b}$$

where γ is a device dependent constant that defines the memristance change rate, and is equal to $\alpha \cdot \mu_V \cdot R_{\mathrm{MIN}} \cdot (R_{\mathrm{MIN}} - R_{\mathrm{MAX}})/D^2$ with confinement of memristance x in $[R_{\mathrm{MIN}}, R_{\mathrm{MAX}}]$.

From (5) and (7b), γ is equal to the second derivative of $f(\hat{q})$ with respect to $\hat{q}$. Thus a charge–flux relationship of the device can be easily found by taking double integrations on γ with respect to $\hat{q}$, as follows:

$$\hat{\varphi} = f_1(\hat{q}) = \iint \gamma \cdot d\hat{q}^2 = \frac{\gamma}{2}\hat{q}^2 + a_1\hat{q} + a_2 \tag{8}$$

where a_1 and a_2 are constant symbols for integrations that depend on the initial condition of the device. Regardless of

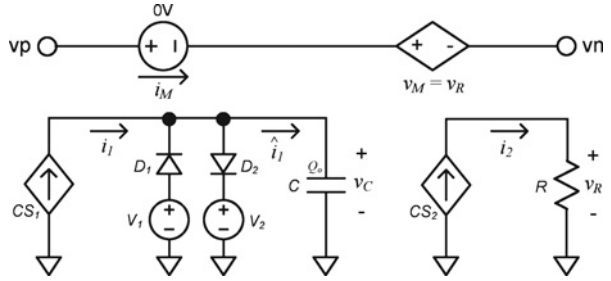

Fig. 3. Compact model for current-controlled memristors, where the dependent current sources of CS_1 and CS_2 produce output currents of $i_1 = i_M$ and $i_2 = R_M(v_C) \times i_1$, respectively. D_1 and D_2 provide a mask function of (3a) on i_1 bypassing the current either when v_C is lower than V_1 or v_C is larger than V_2, so that the v_C can stay at its minimum or maximum value for its hard switching boundary conditions. And thus, v_C becomes equal to the amount of memristive charges scaled by C, regardless of its operating range.

the initial condition, taking shifts from $f_1(\hat{q})$ by $(-a_1/\gamma)$ in $\hat{q}$-axis and by $\left(a_1^2/2\gamma - a_2\right)$ in $\hat{\varphi}$-axis, we arrive at a simple form of the constitutive relationship that is valid in its memristive range as

$$\hat{\varphi} = f(\hat{q}) = \frac{\gamma}{2}\hat{q}^2. \tag{9}$$

Equation (9) can be the base $\hat{\varphi}$-$\hat{q}$ relationship of the memristor, thus a charge-dependent memristance function of $R_M(\hat{q})$ can be found by taking derivatives on (9) with respect to $\hat{q}$, as shown below

$$R_M(\hat{q}) = x(\hat{q}) = \frac{d}{d\hat{q}} f(\hat{q}) = \gamma \cdot \hat{q} \tag{10}$$

where an initial charge amount ($\hat{q}_o$) corresponding to the initial memristance (r_{mo}) can be set as $\hat{q}_o = r_{\mathrm{mo}}/\gamma$. Also the equations (9) and (10) at the secondary boundary condition for $\hat{q}$, i.e., $\hat{q} \in \left[\hat{q}_{\mathrm{MIN}}, \hat{q}_{\mathrm{MAX}}\right]$ lead to

$$\hat{q}_{\mathrm{MIN}} = \min\left(\frac{R_{\mathrm{MIN}}}{\gamma}, \frac{R_{\mathrm{MAX}}}{\gamma}\right), \quad \hat{q}_{\mathrm{MAX}} = \max\left(\frac{R_{\mathrm{MIN}}}{\gamma}, \frac{R_{\mathrm{MAX}}}{\gamma}\right) \tag{11a}$$

and at the boundary values of $\hat{\varphi}$, we have

$$\hat{\varphi}_{\mathrm{MIN}} = \frac{\gamma}{2}\hat{q}_{\mathrm{MIN}}^2, \quad \hat{\varphi}_{\mathrm{MAX}} = \frac{\gamma}{2}\hat{q}_{\mathrm{MAX}}^2. \tag{11b}$$

Fig. 3 shows an equivalent circuit diagram of our compact model for current-controlled memristors, where the dependent current sources CS_1 and CS_2 produce output currents $i_1 = i_M$ and $i_2 = R_M(v_C) \times i_1$, respectively. While v_M can be directly controlled to be equal to $v_M = R_M(v_C) \times i_1$ without use of CS_2 and R, which are included to allow circuit parameter scaling and for cases of more complex $R_M(v_C)$ realization with multiple dependent sources. The ideal diodes D_1 and D_2 represent the mask function (H) on the input current providing bypass current paths at the two boundary resistances. Then the voltage across the capacitor C (v_C) is a time integral of the masked current ($\hat{i}_1$) and thus represents the amount of memristive charges ($\hat{q}$). The current i_2 and thus v_R for a condition of $R = 1\,\Omega$ models (4a). The diodes offer global boundary assurance regardless of the memristor's operation region. For the boundary assurance, V_1 and V_2 in Fig. 3 are set to $\hat{q}_{\mathrm{MIN}}$ and $\hat{q}_{\mathrm{MAX}}$, respectively, along with $C = 1F$ and $R = 1\,\Omega$, so that any excess charge beyond the memristive region can be bypassed through the diodes D_1 and D_2. And thus, the $\hat{q}$ can be safely remain in $\hat{q} \in \left[\hat{q}_{\mathrm{MIN}}, \hat{q}_{\mathrm{MAX}}\right]$ whether the memristor behaves memristively or resistively. The initial charge of the capacitor (Q_o) can be set such that $R_M(Q_o) = r_{\mathrm{mo}}$, where r_{mo} is the initial memristance. On the other hand, it should be noted that the diodes' ON state resistance (r_{on}) strongly affects the simulator's numerical stability. Since it is desirable to be small enough compared to the capacitor impedance while providing strong numerical stability, it is suggested to use a very small value of r_{on} together with scaled C. In our model, small r_{on} of 1 mΩ and scaled C of 1 μF are chosen.

It can be noted that our compact model of Fig. 3, which covers not only the memristor's memristive operation but also its resistive operation, can be easily implemented in most circuit simulators, if not all.

B. Voltage-Controlled Memristors

A generalized representation for a time-invariant voltage-controlled memductive system can be expressed as follows:

$$i_M = G_M(y) \cdot v_M \tag{12a}$$

$$y' = l(y, v_M) \tag{12b}$$

where $G_M(\cdot)$ is an inverse of memristance, i.e., memductance, and y represents internal state variables which incorporate memory effects. For $G_M(y) = y$, the rate function $l(\cdot)$ becomes equal to a memductance change rate. Since the memductance y is a function of flux, i.e., $y = dg(\hat{\varphi})/d\hat{\varphi}$, the rate function $l(\cdot)$ should be equal to the following.

$$y' = \frac{dy}{dt} = \frac{dy}{d\hat{\varphi}} \cdot \frac{d\hat{\varphi}}{dt} = \frac{dy}{d\hat{\varphi}} \cdot \hat{v}_M = \left\{\frac{d^2}{d\hat{\varphi}^2} g(\hat{\varphi})\right\} \cdot \hat{v}_M \tag{13}$$

where $\hat{v}_M$is the masked input voltage by (3b).

While the $g(\hat{\varphi})$function can be found from a separate v–i measurement, we will take it from $f(\hat{q})$ of (9), as an example, by taking an inverse. The inverse is valid for the interested region since $f(\hat{q})$ is a monotonically increasing single valued function within the memristive region, i.e., $\hat{q} \in \left[\hat{q}_{\mathrm{MIN}}, \hat{q}_{\mathrm{MAX}}\right]$

$$\hat{q} = g(\hat{\varphi}) = \sqrt{\frac{2\hat{\varphi}}{\gamma}}. \tag{14}$$

A flux dependent memductance function of $G_M(\hat{\varphi})$ can be found by taking derivatives on (14) with respect to $\hat{\varphi}$

$$G_M(\hat{\varphi}) = y(\hat{\varphi}) = \frac{d}{d\hat{\varphi}} g(\hat{\varphi}) = \frac{1}{\sqrt{2\gamma\hat{\varphi}}} \tag{15}$$

where an initial flux amount ($\hat{\varphi}_o$) corresponding the initial memristance (r_{mo}) can be set as $\hat{\varphi}_o = r_{\mathrm{mo}}^2/2\gamma$. The secondary conditions for $\hat{\varphi}$ and $\hat{q}$ are

$$\hat{\varphi}_{\mathrm{MIN}} = \min\left(\frac{R_{\mathrm{MIN}}^2}{2\gamma}, \frac{R_{\mathrm{MAX}}^2}{2\gamma}\right), \quad \hat{\varphi}_{\mathrm{MAX}} = \max\left(\frac{R_{\mathrm{MIN}}^2}{2\gamma}, \frac{R_{\mathrm{MAX}}^2}{2\gamma}\right) \tag{16a}$$

$$\hat{q}_{\mathrm{MIN}} = \sqrt{\frac{2\hat{\varphi}_{\mathrm{MIN}}}{\gamma}}, \quad \hat{q}_{\mathrm{MAX}} = \sqrt{\frac{2\hat{\varphi}_{\mathrm{MAX}}}{\gamma}}. \tag{16b}$$

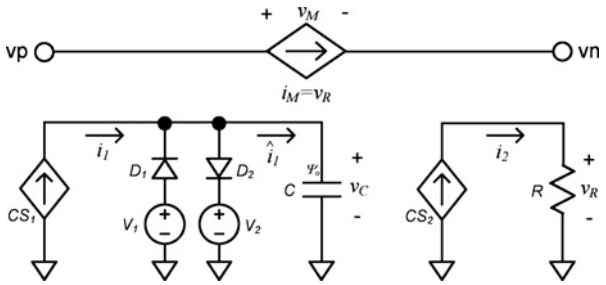

Fig. 4. Model for voltage-controlled memristors. CS_1 and CS_2 produce output currents of $i_1 = v_M$ and $i_2 = G_M(v_C) \times i_1$, respectively. D_1 and D_2 manipulate the mask function of (3b) providing bypass paths at the two boundary resistances, and thus the voltage across the capacitor (v_C) becomes equal to the memristive flux amount scaled by C.

Here, the values of (16a) and (16b) must be same as those of (11b) and (11a), respectively, since they are based on the same constitutive relationship.

From (13) and (15), the rate function, $l(y, v_M)$ can be found by taking additional derivatives on (15) with respect to $\hat{\varphi}$, as follows:

$$l(y, v_M) = \frac{d}{d\hat{\varphi}} G_M(\hat{\varphi}) \cdot \hat{v}_M = -\frac{\hat{\varphi}^{-3/2}}{2\sqrt{2\gamma}} \cdot \hat{v}_M. \qquad (17)$$

Similarly to the current-controlled memristors, a compact model for voltage-controlled memristors is shown in Fig. 4, where the dependent current sources CS_1 and CS_2 produce output currents $i_1 = v_M$ and $i_2 = G_M(v_C) \times i_1$, respectively. The ideal diodes D_1 and D_2 provide bypass paths for the incidents outside the two boundary resistances, and thus the voltage across the capacitor (v_C) which is a time integral of the masked input voltage ($\hat{i}_1 = \hat{v}_M$) becomes equal to the memristive flux amount ($\hat{\varphi}$). The current i_2 and thus v_R for a condition of $R = 1\,\Omega$ models (12a). With $C = 1F$ and $R = 1\,\Omega$, V_1 and V_2 can be set as $\hat{\varphi}_{\rm MIN}$ and $\hat{\varphi}_{\rm MAX}$, respectively, and the initial charge of the capacitor (Ψ_o) can be set to have $G_M(\Psi_o) = 1/r_{\rm mo}$, where $r_{\rm mo}$ is the initial memristance. However, similarly to the current-controlled case, the diodes' ON state resistances ($r_{\rm on}$) are chosen small enough compared to the relatively large impedance of the scaled capacitor.

The macromodel of Fig. 4 covers both memristor's memristive and resistive operations.

V. Parameter Extraction and Simulation Results

In this section, model parameters and simulated results of a voltage-controlled memristor macromodel will be shown, based on the constitutive relationship of (14).

A. Circuit Parameters Extraction

Device related parameters were taken from [1] ($\mu_V = 10^{-10}{\rm cm}^2/{\rm s/V}$, $R_{\rm MIN} = 100\,\Omega$, $R_{\rm MAX} = 20\,{\rm k}\Omega$, and $D = 10$ nm), which rendered a negative valued $\gamma(\approx -59.7 \times 10^9)$ for the scaling factor $\alpha = 300$, whose polarity strongly depends on the device polarity. The negative valued γ means that the memristance will be reduced as the charges (flux) flows from a positive terminal (vp) to the negative terminal (vn), and vice versa. Fig. 5 shows its corresponding log scale $g(\hat{\varphi})$

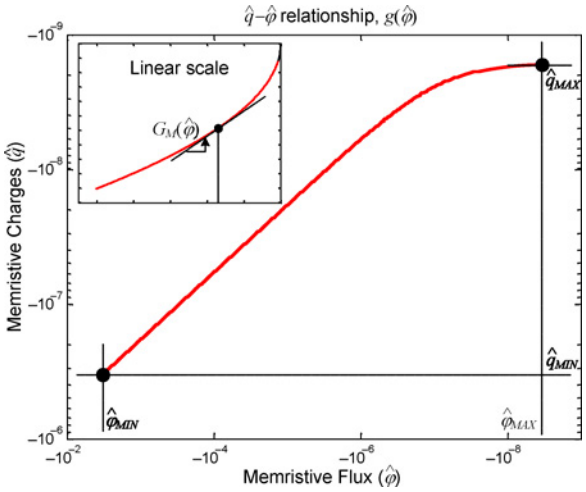

Fig. 5. Memristive charges-flux relationship $g(\hat{\varphi})$ of (14), where the constant γ is $\sim -59.7 \times 10^9 (\hat{\varphi}_{\rm MIN} = -3 \times 10^{-3}$ V·s and $\hat{\varphi}_{\rm MAX} = -0.838 \times 10^{-9}$ V·s).

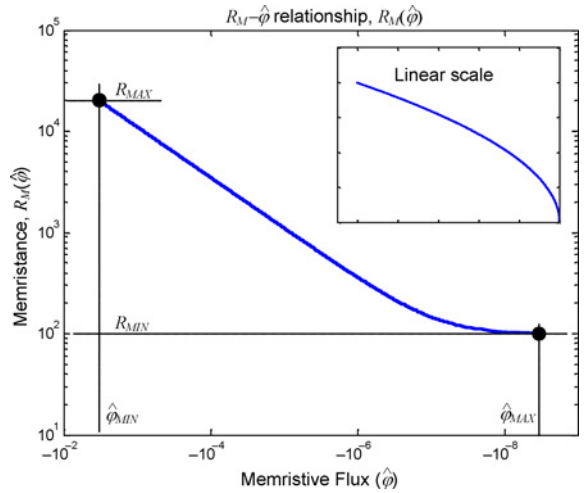

Fig. 6. R_M–$\hat{\varphi}$ relationship, $R_M(\hat{\varphi})$, where the inset is its linear scaled plot and the $R_M(\hat{\varphi})$ is equal to an inverse of $G_M(\hat{\varphi})$ of (15).

function, where the inset is its linear scale plot. $\hat{\varphi}_{\rm MIN}$ and $\hat{\varphi}_{\rm MAX}$ are -3×10^{-3} V·s and -0.838×10^{-9} V·s, respectively. From Fig. 5, we discern that at least ($\hat{\varphi}_{\rm MAX} - \hat{\varphi}_{\rm MIN}$) amount of flux is needed for a full switching of the memristor, from one boundary to the other. Equivalently, ($\hat{q}_{\rm MAX} - \hat{q}_{\rm MIN}$) amount of charges will fully switch the memristance for the current-controlled case. Corresponding to Fig. 5, Fig. 6 shows the log scale R_M–$\hat{\varphi}$ relation, $R_M(\hat{\varphi})$, and the inset is its linear-scale plot, where $R_M(\hat{\varphi})$ is an inverse of $G_M(\hat{\varphi})$.

In circuit realization of $R_M(\hat{\varphi})$ or $G_M(\hat{\varphi})$, any circuit parameters in Fig. 4 can be scaled freely, especially for the gain parameters of CS_1 and CS_2, and for C and R. For the sake of numerical stability of simulators, we selected CS_1 gain (k_1) as 1×10^{-3} and capacitor value (C) as 1mF, which are followed by further scaling on related parameters. Taking Ψ_o with $\hat{\varphi}_o/k_1$ renders the capacitor output voltage with the same value of scaled $\hat{\varphi}$ by (k_1/C)

$$v_C = (k_1/C) \times \left(\hat{\varphi}_o + \int \hat{v}_M \cdot dt\right) = (k_1/C) \times \hat{\varphi}. \qquad (18)$$

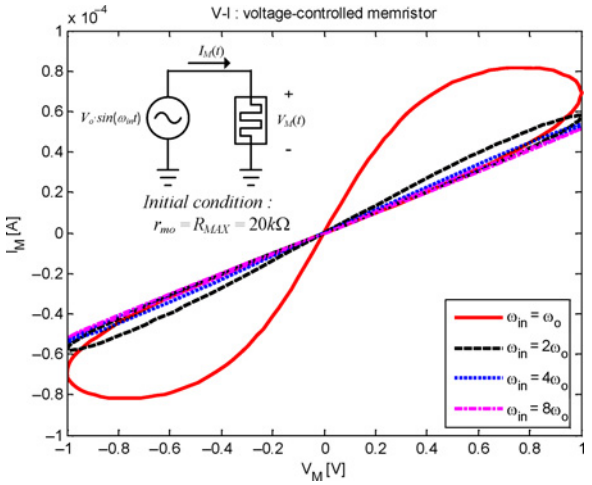

Fig. 7. Simulated momentary v–i behaviors of the voltage-controlled memristor macromodel, where $\omega_o = 2\pi\mu_V/D^2 (f_o = 100$ Hz). Current flowing across the memristor was measured for a sinusoidal voltage input, $v_M(t) = 1 \cdot \sin(\omega_{in}\, t)$, as the test condition shown in the inset.

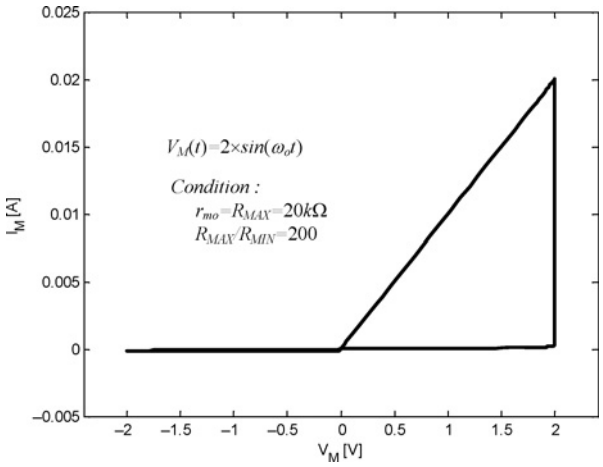

Fig. 8. v–i behaviors for $v_M(t) = 2 \cdot \sin(2\pi f_{in} t)$, where the input frequency of $f_{in} = f_o = 100$ Hz and $R_{\mathrm{MAX}}/R_{\mathrm{MIN}} = 200$.

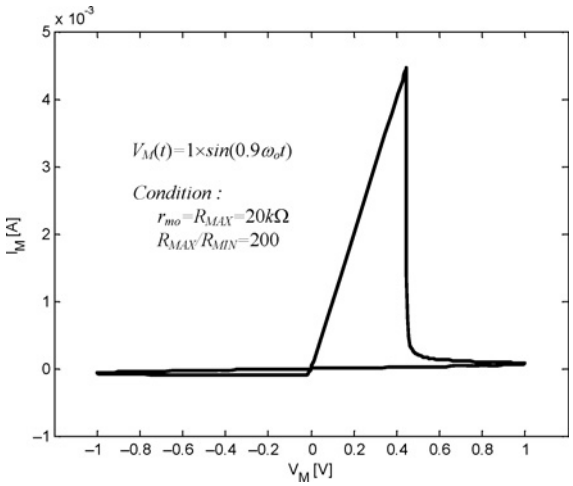

Fig. 9. v–i behaviors for $v_M(t) = 1 \cdot \sin(2\pi f_{in} t)$, where the input frequency of $f_{in} = 0.9 \times f_o = 90$ Hz and $R_{\mathrm{MAX}}/R_{\mathrm{MIN}} = 200$.

Regarding the v_C scaling in (18), V_1 and V_2 are also scaled to

$$V_1 = (k_1/C) \times \hat{\varphi}_{\mathrm{MIN}}, \quad V_2 = (k_1/C) \times \hat{\varphi}_{\mathrm{MAX}}$$

and when i_2 is produced by CS_2 as $i_2 = G_M(v_C \times C/k_1) \times i_1$, it is equivalent to $i_2 = G_M(\hat{\varphi}) \times (v_M \cdot k_1) = k_1 \times \{G_M(\hat{\varphi}) \cdot v_M\}$. Finally, with R scaling ($R = 1/k_1 = 1k\Omega$), the voltage across the resistor (v_R) becomes equal to the memristor's output current, $v_R = i_2 \times R = G_M(\hat{\varphi}) \cdot v_M$.

By putting v_R for the unity-gain dependent-current source, a compact model of the voltage-controlled memristors can be established.

B. Simulation Results With the Macromodel

With the parameters extracted in the previous section, a voltage-controlled memristor model was developed in Spectre for the following circuit simulations.

Among the several properties of the memristive systems which were identified by Chua and Kang [15], the most distinct property is the zero-crossing property: the output v_M (or i_M) is always zero whenever the input i_M (or v_M) is zero regardless of the internal state variables x (or y) and R_M (or G_M), as it can be expected from (4) and (12). This property will be manifested in the pinched hysteretic v–i characteristics for a periodic balanced input. Also, it is notable that the memristor behaves as a linear resistor in the limit of infinite frequency at which there is no response time allowed to produce resistance change during the short input period.

The simulated transient v–i characteristics of the voltage-controlled memristor model, for sinusoidal voltage inputs, i.e., $v_M(t) = 1 \cdot \sin(\omega_{in} t)$, are shown in Fig. 7, where the current flowing across the memristor was measured for the inputs with different frequencies. The pinched hysteretic loops clearly appear at low frequencies which are collapsed to that of a linear resistor at high frequencies, implying that our model is valid satisfying basic properties of the general memristive systems [14], [15]. For the fully balanced periodic input, the memristance behaves also periodic over the input period, since the injected amount of net flux over each period is equal to zero. It can also be noted that the range of memristance change is strongly dependent on the input frequency and amplitude, because the amplitude of flux pattern is linearly proportional to the input voltage amplitude and inversely proportional to the input frequency.

In Fig. 7, it should be noted that the input frequency and the voltage amplitude were chosen for the memristance not to exhibit the full memristance range between R_{MIN} and R_{MAX}. However, when the input amplitude was doubled at a frequency of ω_o, $v_M(t) = 2 \cdot \sin(\omega_o t)$, to provide a full switching condition, the memristor behaved differently in its v–i characteristics as shown in Fig. 8. Fig. 9 shows another hard switching condition with lowered input frequency ($\omega_{in} = 0.9 \times \omega_o$) under the unit amplitude ($V_O = 1$-V). The behaviors similar to those in Figs. 8 and 9 for hard switching cases, as already reported in [1], are caused by the nonlinear characteristics of the flux-dependent memristance change rate, i.e., a very high rate for small memristances and a low rate for large memristances. All of the v–i characteristics of our memristor model, shown in Figs. 7–9, verify that our model successfully

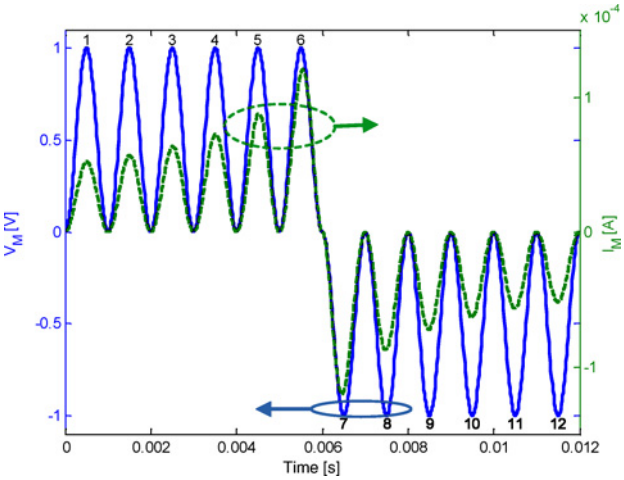

Fig. 10. Unbalanced input voltage waveform (solid) and its corresponding output current waveform (dashed).

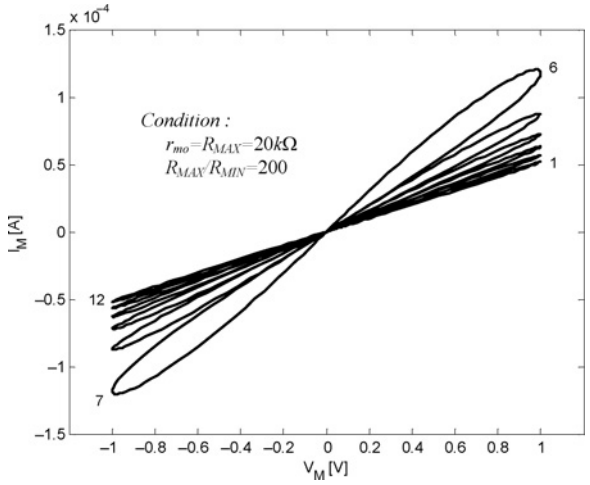

Fig. 11. v–i behaviors corresponding to the waveforms in Fig. 10, where the memristance keep increasing or decreasing for the same input polarity.

reproduce memristor's nonlinear behaviors reported in [1], regardless of whether the memristor is in its memristive region or in resistive region at boundary memristances.

For a balanced voltage input, memristors exhibit negligible memristance changes at high frequencies and thus can be treated as static linear resistors [14], [15]. However, if the input is unbalanced, the memristance will change even at high-input frequencies, since even the net flux will be accumulated over time and eventually will affect the memristance. Fig. 10 shows examples of unbalanced voltage input and its corresponding current output waveforms, where the input is patterned as $v_M(t) = +\sin^2(5w_O t)$ for the first six periods, and as $v_M(t) = -\sin^2(5w_O t)$ for the next six periods. The output current waveform is no longer periodic over the periodic unbalanced high-frequency input. Its corresponding momentary v–i characteristics are depicted in Fig. 11, showing that memristance tends to keep increasing or decreasing unless the input polarity is negated, even with the relatively high-input frequency of $5w_O$. It should be noted that the amount of memristance change can be uniquely determined by the memristive flux amount, as expected from (15), which is linearly dependent on the input frequency and amplitude.

From the results shown in this section, it can be confirmed that our simple models with bypass current paths through diodes, shown in Figs. 3 and 4, provide global boundary assurance whether memristors behave memristively or resistively. Our model can be easily implemented in circuit simulators such as SPICE, Spectre, and Verilog-A.

VI. Discussion

A. Dependency of Models on Types of Excitation Signal

The compact models described in Section IV are basically composed of resistorless ports that should be driven by a specific type of input signal according to their port configurations: current driven current-controlled memristor model, and voltage driven voltage-controlled one. However, those resistorless models can cause practical problems in simulating their application circuits, due to the well-known conflict of voltage sources in the loop or current sources in series [12]. For example, usage of the current-controlled model of Fig. 3 is limited for current driving cases only. Though the classification of memristors to current and voltage-controlled types has primarily a methodological importance in describing and device modeling, a concrete practical memristor model is desirable to be controlled either by current or voltage.

This problem has been recently discussed in a previous work by Biolek *et al.*, where they presented that the problem can be avoided by a case-by-case utilization of a specific form of port equations (12). For an example of our current-controlled model of Fig. 3, its dependency on excitation types can be resolved by simply forming the memristive port (between vp and vn) with a variable resistor only whose value is determined by a equation $R_M(v_C)$, omitting CS_2 and R. The boundary assurance is being kept by the bypass paths through D_1 and D_2.

B. Consideration of Nonlinear Dopant Drift Effect

While the (6a) and (6b) were proposed in [1], the authors proposed to use an appropriate window function on the rate function of state variables, (6b), to model so called 'nonlinear dopant drift effect' that was expected from their experimental measurements of physical TiO_2 thin film devices [1]. The nonlinear drift effect causes nonconstant change rate of state variables over their available range showing much lower speed around the two boundaries compared to the mid range. Recent work by Joglekar *et al.* [13] proposed a window function of $\{1-(2x-1)^{2p}\}$, where the normalized state variable x is limited in [0, 1], and p is a positive integer. The Joglekar window ensures that the change rate of the state variable gradually decreases as the variable approaches to two boundary values. However, due to the zero drift at the boundaries, the window function may cause another practical problem that it may not be back to memristive operation forever once it arrives at either of boundaries [11]. In order to avoid the backing problem, [11] has proposed a modified window function that sets the state variable change rate at a boundary to a nonzero value when the input polarity is negated. However, the modified window

function with the dynamically selectable change rate of the state variable depending on the input signal polarity will be fail to offer a clearly definable constitutive relationship.

As described in Section III, our modeling approach is grounded on the constitutive relationship between charge and flux-linkage across the memristor which can be uniquely provided by any memristor. In fact, our approach does not require any special window function for the nonlinear drift effect, since the measured constitutive relationship reflects all kind of device characteristics including the nonlinear drift effect. Paradoxically, any addition of window function to the state variable change rate which was originally derived from the constitutive relationship will yield a modified constitutive relationship. However, when we need to model memristors whose constitutive relationship cannot be physically measured and the memristance change rate is nonconstant, a similar type of window function reported in [11], [13] can be considered in the right side of (7b). Since our models shown in Figs. 3 and 4 already hold boundary assurance offered by the two diodes, a window function with nonzero value (δ) even at boundaries can be used to avoid the backing problem from the boundaries, such as

$$W(\hat{q}) = \delta + \left\{ 1 - (2\hat{z} - 1)^{2p} \right\} \tag{19}$$

where δ is a positive constant ($\delta \ll 1$) and $\hat{z}$ is a normalized memristive charge, i.e., $\hat{z} = (\hat{q} - \hat{q}_{\mathrm{MIN}}) / (\hat{q}_{\mathrm{MAX}} - \hat{q}_{\mathrm{MIN}})$. The small nonzero value of δ at boundaries guarantees the model can be back to the memristive from the resistive region as soon as the input polarity is negated. When the window function of (19) is included in (7b), it will also update the constitutive relationship between charges and flux, as follows, since the memristance change rate becomes equal to $\gamma \cdot W(\hat{q})$

$$\hat{\varphi} = f_1(\hat{q}) = \iint \gamma \cdot W(\hat{q}) \cdot d\hat{q}^2. \tag{20}$$

Once a shifted constitutive relationship is chosen from (20), the remaining modeling procedure is exactly the same as the linear drift model case shown in Section IV. In summary, the nonlinear drift effect can be modeled without any residual problem from the boundary limiting cases by using the window function of (19), while preserving its assurance provided by the bypass diodes in Figs. 3 and 4.

VII. Conclusion

A compact modeling method for memristors based on the constitutive relationship between charge and flux has been introduced. For memristors with limited resistance ranges, we discussed how the constitutive relationship can be defined, and then developed our compact models for current-controlled and voltage-controlled memristors. The models have matched successfully the HPs numerical model, satisfying all of memristors' observed properties. Our compact models uniquely provide the boundary assurance, thus are valid globally whether memristors behave memristively or resistively. In addition, we have discussed how to avoid a practical limitation of our models for specified type of driving signals, along with adoption of a potential window function for nonlinear drift effect modeling.

References

[1] D. B. Strukov, G. S. Snider, D. R. Stewart, and R. S. Williams, "The Missing Memristor Found," *Nature*, vol. 453, pp. 80–83, May 2008.

[2] J. J. Yang, M. D. Pickett, X. Li, D. A. Ohlberg, D. R. Stewart, and R. S. Williams, "Memristive switching mechanism for metal/oxide/metal nanodevices," *Nat. Nanotechnol.*, vol 3, no. 7, pp. 429–433, 2008.

[3] R. Waser and M. Aono, "Nanoionics-based resistive switching memories," *Nature Materials*, vol. 6, no. 11, pp. 833–840, 2007.

[4] P. Kuekes, "Material Implication: Digital logic with memristors," in *Proc. Memristor Memristive Syst. Symp.*, Nov. 2008.

[5] D. B. Strukov and K. K. Likharev, "CMOL FPGA: A reconfigurable architecture for hybrid digital circuits with two-terminal nanodevices," *Nanotechnology*, vol. 16, no. 6, pp. 888–900, Jun. 2005.

[6] G. S. Snider, "Self-organized computation with unreliable, memristive nanodevices," *Nanotechnology*, vol. 18, no. 36, p. 13, Sep. 2007.

[7] K. Likharev, A. Mayr, I. Muckra, and O. Turel, "CrossNets: High-performance neuromorphic architectures for CMOL circuits," *Ann. N. Y. Acad. Sci.*, vol. 1006, pp. 146–163, Dec. 2003.

[8] G. S. Snider, "Memristors as synapses in a neural computing architecture," in *Proc. Memristor Memristive Syst. Symp.*, Nov. 2008.

[9] Y. V. Pershin, S. L. Fontaine, and M. D. Ventra, "Memristive model of amoeba's learning," in *Proc. Nature*, Oct. 2008 [Online]. Available: http://hdl.handle.net/10101/npre.2008.2431.1

[10] S. Shin, K. Kim, and S. M. Kang, "Memristor-based fine resolution resistance and its applications," in *Proc. Int. Conf. Commun., Circuits, Syst.*, Jul. 2009, pp. 948–951.

[11] Z. Biolek, D. Biolek, and V. Biolkova, "SPICE model of memristor with nonlinear dopant drift," *Radioengineering*, vol. 18, no. 2, pp. 210–214, Jun. 2009.

[12] D. Biolek, Z. Biolek, and V. Biolkova, "SPICE modeling of memristive, memcapacitative, and meminductive systems," in *Proc. Eur. Conf. Circuit Theory Design*, Aug. 2009, pp. 249–252.

[13] Y. N. Joglekar and S. J. Wolf, "The elusive memristor: Properties of basic electrical circuits," *Eur. J. Phys.*, vol. 30, no. 4, pp. 661–675, 2009.

[14] L. O. Chua, "Memristors: The missing circuit element," *IEEE Trans. Circuit Theory*, vol. 18, no. 5, pp. 507–519, Sep. 1971.

[15] L. O. Chua and S. M. Kang, "Memristive devices and systems," *Proc. IEEE*, vol. 64, no. 2, pp. 209–223, Feb. 1976.

[16] M. D. Ventra, Y. V. Pershin, and L. O. Chua, "Circuit elements with memory: Memristors, memcapacitors, and meminductors," *Proc. IEEE*, vol. 97, no. 10, pp. 1717–1724, Oct. 2009.

Sangho Shin (S'02–AM'08–M'10) received the B.S. degree from the Korea Aerospace University, Gyeonggi-do, in 2000, and M.S. and Ph.D. degrees from the Korea Advanced Institute of Science and Technology (KAIST), Daejeon, in 2002 and 2007, respectively, all in electrical engineering.

Prior to joining UC Merced in August 2007, he was with PHYCHIPS, Inc., Daejeon, Korea, as a Senior Integrated Circuit (IC) Design Engineer worked on analog and mixed-signal ICs and radio frequency (RF) front-end blocks for 5.8 GHz dedicated short range communication and mobile radio frequency identification reader products. From 2001 to 2004, he was with Micro Information and Communication Remote Object-oriented Systems Research Center, KAIST, where he worked toward the low-power implementation of mixed-mode and radio integrated circuits for low-rate wireless personal area network (LR-WPAN) systems. From 2004, he conducted a two year research collaboration with the UC Santa Cruz, where he developed an energy efficient RF complementary metal oxide semiconductor ICs for low-power wireless communication systems. He is currently with the School of Engineering, University of California (UC) Merced, as a Post-Doctoral Researcher, researching broadly on the elusive memristive devices and systems exploiting their useful applications and compact models. His current research interests include low-power analog/RF integrated circuits; low-power very large scale integration design; mixed-signal mixed-technology integrated system; modeling and simulation of semiconductor devices and circuits; high-speed input/output schemes; analysis and estimation of 3-D thermal distribution.

Kyungmin Kim (S'04–AM'08) received the B.S. degree in information and telecommunication engineering from Korea Aerospace University, Gyeonggi-do, the M.S. degree in information and communication engineering from the Gwangju Institute of Science and Technology, Gwangju, Korea, and the Ph.D. degree in electrical engineering from KAIST, in 2000, 2002, and 2007, respectively.

Currently, she is with the School of Engineering, UC Merced, as a Post-Doctoral Researcher, working on analysis of memristive systems, secure chaotic communications, and the neuromorphic signal processing. Her research interests include wireless communications, which include space-time codes, multiple input multiple output systems, and the related signal processing.

Sung-Mo (Steve) Kang (S'73–M'75–SM'80–F'90) received the B.S. degree from Fairleigh Dickinson University, Teaneck, NJ in 1970, the M.S. degree from the State University of New York at Buffalo in 1972, and the Ph.D. degree from the University of California Merced, Merced, in 1975, all in electrical engineering.

From 1995 to 2000, he was the Head of the Department of Electrical and Computer Engineering, University of Illinois at Urbana-Champaign (UIUC). Prior to UIUC, he was a Supervisor of High-End Microprocessor Design with AT&T Bell Laboratories, Murray Hill, NJ, and also has served as a Faculty Member of Rutgers University, New Brunswick, NJ. He was a Visiting Professor at the University of Karlsruhe in 1997, the Technical University of Munich in 1998, KAIST in 2003, and the Swiss Federal Institute of Technology, Lausanne, in 1989 and 2006. From 2001 to 2007, he was the Dean of Baskin School of Engineering and Professor of Electrical Engineering at UC Santa Cruz. He is currently the Chancellor and Professor of Engineering with the School of Engineering, UC Merced. He holds 15 patents, published over 350 papers, and co-authored nine books. His research interest includes low-power very large scale integration design; mixed-signal mixed-technology integrated system; modeling and simulation of semiconductor devices and circuits; high-speed optoelectronic circuits and systems; and bioelectronic circuits and systems.

Dr. Kang has served on the Editorial Boards of the PROCEEDING OF THE IEEE, the IEEE TRANSACTIONS ON CIRCUITS AND SYSTEMS, the *International Journal of Circuit Theory and Applications*, and *Circuits, Signals and Systems*, as the Founding Editor-in-Chief of the IEEE TRANSACTIONS ON VERY LARGE SCALE SYSTEMS and as the President of the IEEE Circuits and Systems (CAS) Society in 1991. He was inducted into the Silicon Valley Engineering Council Hall of Fame in 2009. He is the recipient of the IEEE Circuits and Systems Society Meritorious Service Award in 1994, the Humboldt Research Award for Senior U.S. Scientists in 1996, the IEEE Graduate Teaching Technical Field Award in 1996, the IEEE CAS Society Technical Achievement Award in 1997, the Korean Broadcasting System Award in Industrial Technology in 1998, the Semiconductor Research Corporation Technical Excellence Award in 1999, the IEEE CAS Society Golden Jubilee Medal in 1999, the IEEE Third Millennium Medal in 2000, the Outstanding Alumnus Award in Electrical Engineering, UC Berkeley, in 2001, the Mac E. Van Valkenburg Society Award of IEEE Circuits and Systems Society in 2005, the Chang-Lin Tien Education Leadership Award in 2007, the International Society for Quality Electronic Design Quality Award in 2008, and the Korean-American Leadership Award in 2008. He is a Fellow of the Association for Computing Machinery and the American Association for the Advancement of Science.